THE JOURNAL OF PHYSICAL CHEMISTRY LETTERS
A JOURNAL OF THE AMERICAN CHEMICAL SOCIETY

pubs.acs.org/JPCL

Letter

Work Function Engineering of 2D Materials: The Role of Polar Edge Reconstructions

Guoxiang Hu,* Victor Fung, Jingsong Huang, and P. Ganesh*

Cite This: *J. Phys. Chem. Lett.* 2021, 12, 2320−2326

Read Online

ACCESS | Metrics & More | Article Recommendations | Supporting Information

ABSTRACT: 2D materials have attracted tremendous interest as functional materials because of their diverse and tunable properties, especially at their edges. A material's work function is a critical parameter in many electronic devices; however, a fundamental understanding and a path toward large alterations of the work function in 2D materials still remain elusive. Here, we report the first evidence for anisotropy of the work function in 2D MoS_2 from first-principles calculations. We also demonstrate large work-function tunability (in the range of 3.45−6.29 eV) choosing the 2H phase of MoS_2 as a model system by sampling various edge configurations. We furthermore reveal the origin of this work function anisotropy and tunability by extending the existing work function relation to the local dipole moment at surfaces of 3D materials to those at edges in 2D materials. We then use machine-learning approaches to correlate work function with edge structures. These results pave the way for intrinsic edge engineering for electronic and catalytic applications.

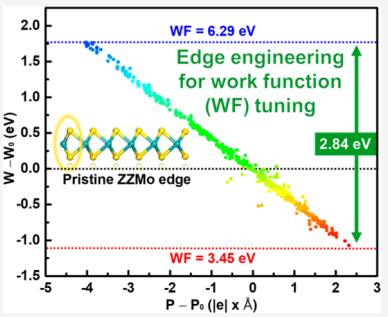

Atomically thin two-dimensional (2D) materials ranging from metallic graphene, semiconducting transition-metal dichalcogenides (TMDCs), to highly insulating hexagonal boron nitride have attracted widespread research interest over the past decade.[1−4] Because of their exceptional physical and chemical properties, they have been widely used as components in various electronic devices.[5−8] Work function, which is the minimum energy needed to remove an electron from a solid to a point in the vacuum immediately outside the solid surface, is a crucial parameter for the design of electron emitters, photovoltaic devices, and electrocatalysts.[9−13] Consequently, numerous research efforts have been made to modify the work function of 2D materials to improve device performance.[14−17] For example, by immersing the graphene films into $AuCl_3$ solution, the work function of graphene was adjusted by 0.5 eV, allowing the power conversion efficiency of the photovoltaic device to be improved by 40 times.[18] In addition, by varying the environment from vacuum to O_2, a work function variation of 0.43 eV in MoS_2 monolayer was achieved, thereby enabling a high-quality homojunction diode with partial passivation.[19] However, fundamental understandings of factors that control the work function in 2D materials, the degree of tunability of work function at the 2D limit, as well as practical ways of achieving this tunability for various nanoscale applications/devices remain to be developed.

The work function (W) of a 3D material can be written as $W = -e\Phi - E_F$, where the first term is precisely the energy to overcome the surface dipole barrier, approaching a constant at distances far from the surface, and the second term is the energy of the Fermi level of the bulk, from which the electron is removed.[20] The surface dipole barrier is formed because of (a) the redistribution of the electron density on the surface due to the termination of periodic boundary condition and (b) ionic reconstruction of the surface that gives rise to a different atomic arrangement on the surface compared to the bulk; hence, the surface dipole barrier is naturally different for different surfaces or surface reconstructions, both for metals and semiconductors. It is well-known that the work function of 3D materials is surface-dependent and anisotropic, although the variability that one can obtain is not too high.[21−23] The definition of work function in 3D materials is immediately not evident in 2D materials, because there is no clear distinction between bulk and surface atoms in 2D materials. It is also not clear what will be the 2D limit of the work function anisotropy, where two types of surfaces (2D planar surfaces and 1D edges) coexist.

We assume that edge atoms in 2D materials are analogous to surface atoms in 3D materials, while surface atoms in 2D materials are analogous to bulk atoms in 3D materials. On the basis of this interpretation, the work functions of edges in 2D materials can be obtained. In addition to the conventional zigzag or armchair edges common to hexagonal 2D materials, more complex edge reconstructions have been synthesized and demonstrated to show functional properties.[24,25] We have shown that there is indeed a wide family of synthesizable, reconstructed edges in 2D TMDCs, with many potential

Received: January 26, 2021
Accepted: February 23, 2021
Published: March 2, 2021

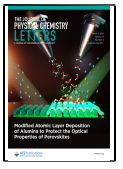

https://dx.doi.org/10.1021/acs.jpclett.1c00278
J. Phys. Chem. Lett. 2021, 12, 2320−2326

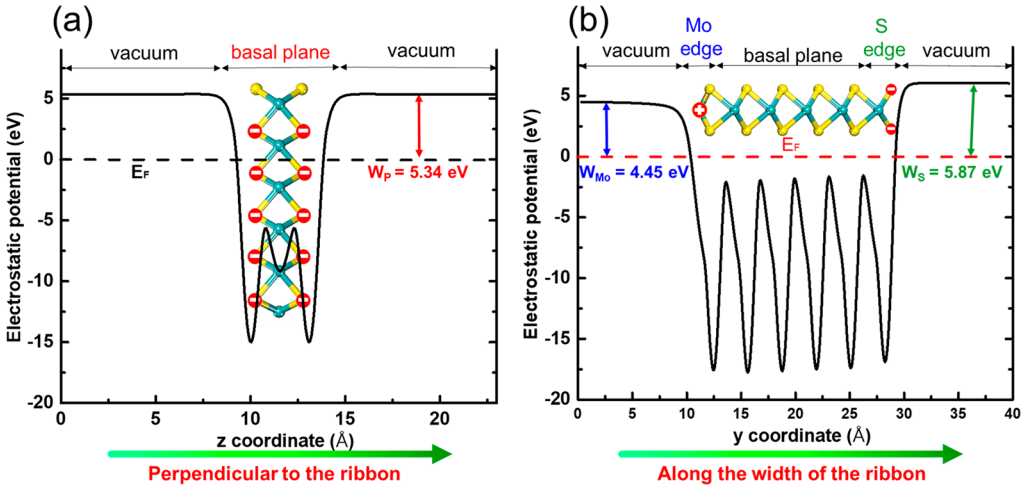

Figure 1. Plane-averaged electrostatic potential energy of a pristine MoS_2 nanoribbon (a) along the normal direction and (b) along the in-plane direction. The Fermi level (E_F, which is set at 0 eV) and the work function perpendicular to the ribbon (W_P), the work functions along the width of the ribbon at the Mo side (W_{Mo}), and at the S side (W_S) are indicated by the dashed line and red, blue, and green double-headed arrows, respectively. The structure of the nanoribbon is also shown (Mo, cyan; S, yellow).

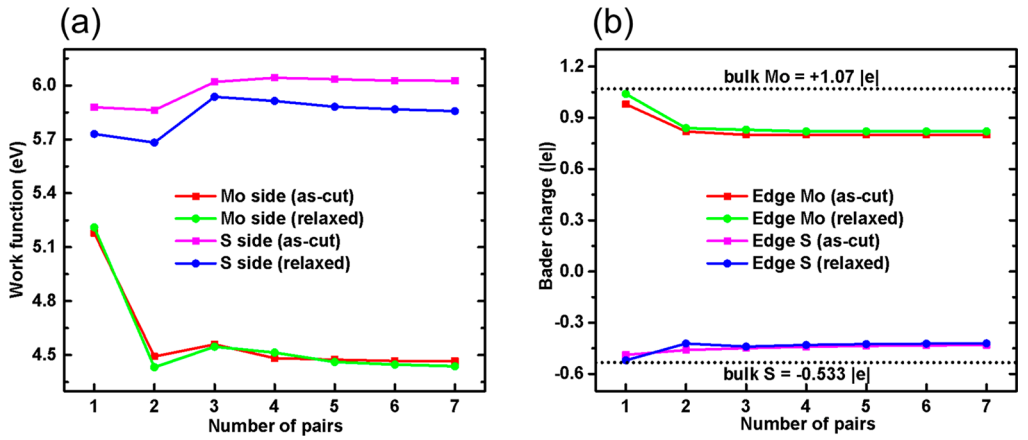

Figure 2. (a) Work functions along the width of the ribbon at the Mo and S sides as a function of the ribbon width in terms of the number of Mo and S pairs. (b) Bader charges on the edge Mo and edge S as a function of the ribbon width. Dashed lines indicate the Bader charges for Mo and S atoms in 2H MoS_2, i.e., bulk of 2D monolayer material.

nanoscale applications.[26,27] Therefore, the edge reconstructions of 2D materials may offer a new opportunity for work function modification as a result of the possibly different barrier energies at the edges. In this work, using first-principles density functional theory (DFT), we attempt to investigate if the work function of 2D materials can be effectively tuned by edge reconstructions, to what degree it can be tuned, and what underlying mechanism is responsible for this tunability. We choose the well-studied 2H MoS_2 as a representative example to explore this question. The approach of investigation we lay out in this Letter can be straightforwardly expanded to other 2D materials in the future. We first study the anisotropy of the work function in the pristine MoS_2 nanoribbons. Next we investigate the 3 most stable reconstructed edges at different Mo/S ratios (Mo-rich, stoichiometric, and S-rich) and then screen a wide structural space with 625 edge configurations. At last, we reveal the origin of the work function anisotropy and tunability.

To understand the anisotropy of the work function in 2D materials, we used a nanoribbon model with metallic zigzag edges constructed based on the well-studied 2H MoS_2. We computed the work function by comparing the vacuum level with the Fermi level, namely, $W = E_{VAC} - E_F$. For the same nanoribbon, the Fermi level is a constant, so the work function depends on the local vacuum level. The local vacuum level can be obtained from the electrostatic potential energy that uses an electron as the test charge. We plotted the plane-averaged electrostatic potential energy of a pristine 2H MoS_2 nanoribbon with 6 pairs of Mo and S rows (width ≈ 14.55 Å). We found that the work function is 5.34 eV along the normal direction (Figure 1a). However, along the width of the ribbon, the work function is 4.45 eV at the Mo side and 5.87 eV at the S side (Figure 1b). This indicates that the work function of 2D materials is orientation-dependent, similar to that of 3D materials as noted above. The anisotropy of the work function in 2D materials has been conventionally overlooked. In most cases only the work function along the normal direction has been considered, while experimental advances in making devices with stacked 2D materials make studying the anisotropy highly relevant. Indeed, 2D TMDC films with vertically aligned layers have been successfully synthesized, showing improved field emission, gas adsorption, and catalytic properties.[28−31] A modulation of work function as large as 0.89 eV (5.34 eV − 4.45 eV) is realized simply by changing the

https://dx.doi.org/10.1021/acs.jpclett.1c00278
J. Phys. Chem. Lett. 2021, 12, 2320−2326

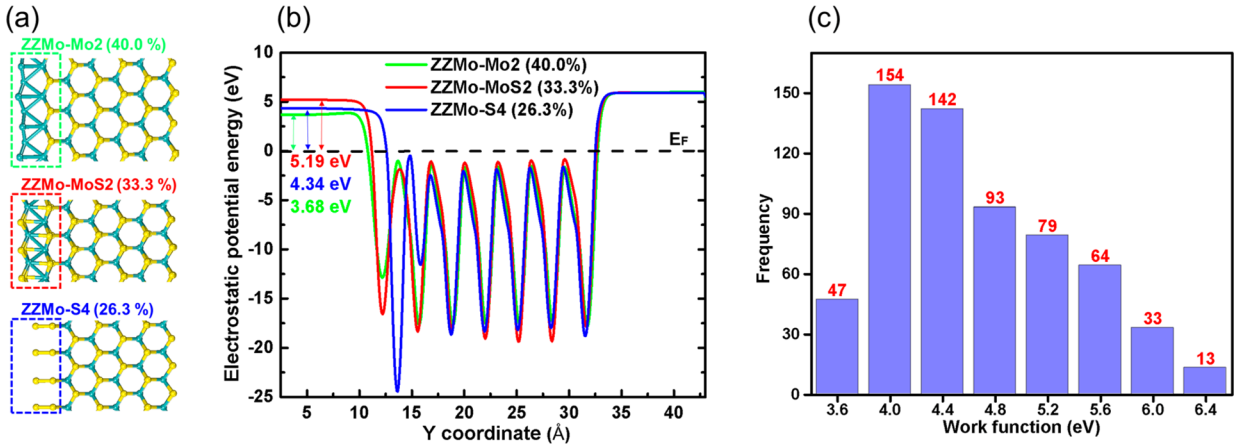

Figure 3. (a) Geometric structures of three MoS_2 nanoribbons with reconstructed edges at the Mo (left) side. Mo, cyan; S, yellow. (b) Plane-averaged electrostatic potential energy of the nanoribbons. The Fermi level (E_F, which is set at 0 eV) and the work function of ZZMo-Mo2, ZZMo-MoS2, and ZZMo-S4 are indicated by the dashed line and green, red, and blue double-headed arrows, respectively. (b) Histogram of the work function at the Mo side along the width of the ribbon for the 625 nanoribbons.

orientation of a single 2D MoS_2 nanoribbon. It is noteworthy that the difference in the work function between the two edges is even larger with a value of 1.42 eV (5.87 eV − 4.45 eV).

It is known that the width of the nanoribbon plays an important role in its electronic structure.[32−34] Therefore, we investigate how the work function of the MoS_2 nanoribbon is affected by the ribbon width. Figure 2a shows the work functions along the width of the ribbon at the Mo and S sides as a function of the ribbon width. It is noted that the Fermi level of the nanoribbon changes when the ribbon width changes, and the work functions were obtained by comparing the vacuum level with the Fermi level for each individual nanoribbon. As one can see, the work functions at both sides are converged (within 0.015 eV) when the ribbon width is larger than 5 pairs (∼11.82 Å). Effects of local atomic relaxations at the edges are observed to be relevant mainly for the S side and also converge quickly with the size of ribbon width. This indicates that the interactions between the two sides of the ribbon are very weak when the ribbon width is larger than 11.82 Å. We also calculated the Bader charges on the edge Mo and edge S atoms (Figure 2b), which turn out to be also converged (within 0.02lel) at the same ribbon width. Compared to the values for the 2D monolayer, the Bader charges of Mo and S atoms at the edges are slightly reduced in magnitude but remain to be positively and negatively charged as a result of their different electronegativities. Thus, the reason behind the significant difference in the work function at the two edges of the nanoribbon as shown above can be explained by their charge distributions. Although the Fermi level is constant throughout the nanoribbon, the negatively charged edge S leads to a negative dipole (pointing inward) and a larger work function at the S edge, while the positively charged edge Mo causes a smaller work function at the Mo edge.

Next we turn to nanoribbons with reconstructed edges, as studied earlier in various experiments as well as computations.[24−26,35] Here we mainly consider edge reconstructions at the Mo side, but the methodology developed here for the Mo side can be easily extended to the S side, which would be also of interest to study in the future. We set the ribbon width to 5 pairs to avoid strong interactions between the two sides of the ribbon (Figure 2a). Following our previously developed workflow,[26] we generated 625 edge configurations from tiling the triangular lattice. It is noted that with edge reconstructions all the nanoribbons remain metallic (at the edges), with 41 nanoribbons becoming half-metallic. The metallic/half-metallic characters of the edges can increase the electrical conductivity in electrocatalysis and photocatalysis. In addition, the highly localized electron states at the edges have the ability to donate and accept electrons and thus can act as catalytic sites just like ordinary metal surfaces. This could be of general importance, providing a route for the hydrotreating catalysis.[36]

We first illustrate the effect of edge reconstructions with the most stable Mo-rich, stoichiometric, and S-rich reconstructed edges. The geometric structures and plane-averaged electrostatic potential energies of the three nanoribbons are shown in panels a and b of Figure 3, respectively. The edges are labeled based on the orientation and composition of the outermost termination group, with the percentage of Mo in each nanoribbon shown in the bracket. We find the work functions at the S side of the 3 ribbons are the same (5.87 eV), owing to the large distance and negligible interactions between the two sides of the ribbons, and thus unchanged local dipole moment. As such we use the vacuum level of the S side of the ribbon as a reference as shown in Figure 3b. We find the reconstructed stoichiometric edge ZZMo-MoS2 has a work function of 5.19 eV, followed by the S-rich edge ZZMo-S4 (4.34 eV) and the Mo-rich edge ZZMo-Mo2 (3.68 eV). Compared with the pristine edge, the work function can be tuned by +0.74 eV (5.19 eV − 4.45 eV) in the case of ZZMo-MoS2 and by −0.77 eV (3.68 eV − 4.45 eV) in the case of ZZMo-Mo2. Then we extend this analysis to all of the 625 reconstructed edges. The histogram of the work functions at the Mo side is shown in Figure 3c. Excitingly, we find that a wide range of work functions from 3.45 to 6.29 eV can be achieved from the 625 edge configurations, with almost ∼3 eV of tunability. This is the largest difference ever reported, indicating that the work function can be effectively tuned by edge reconstructions. Histograms of the work function at the S side and along the normal direction for the 625 structures examined here are shown in Figure S1. As one can see, the work function at the S side remained practically unchanged owing to the large ribbon width.

To explore the potential relationships between the chemical properties of the edges and their work function, we first

https://dx.doi.org/10.1021/acs.jpclett.1c00278
J. Phys. Chem. Lett. 2021, 12, 2320−2326

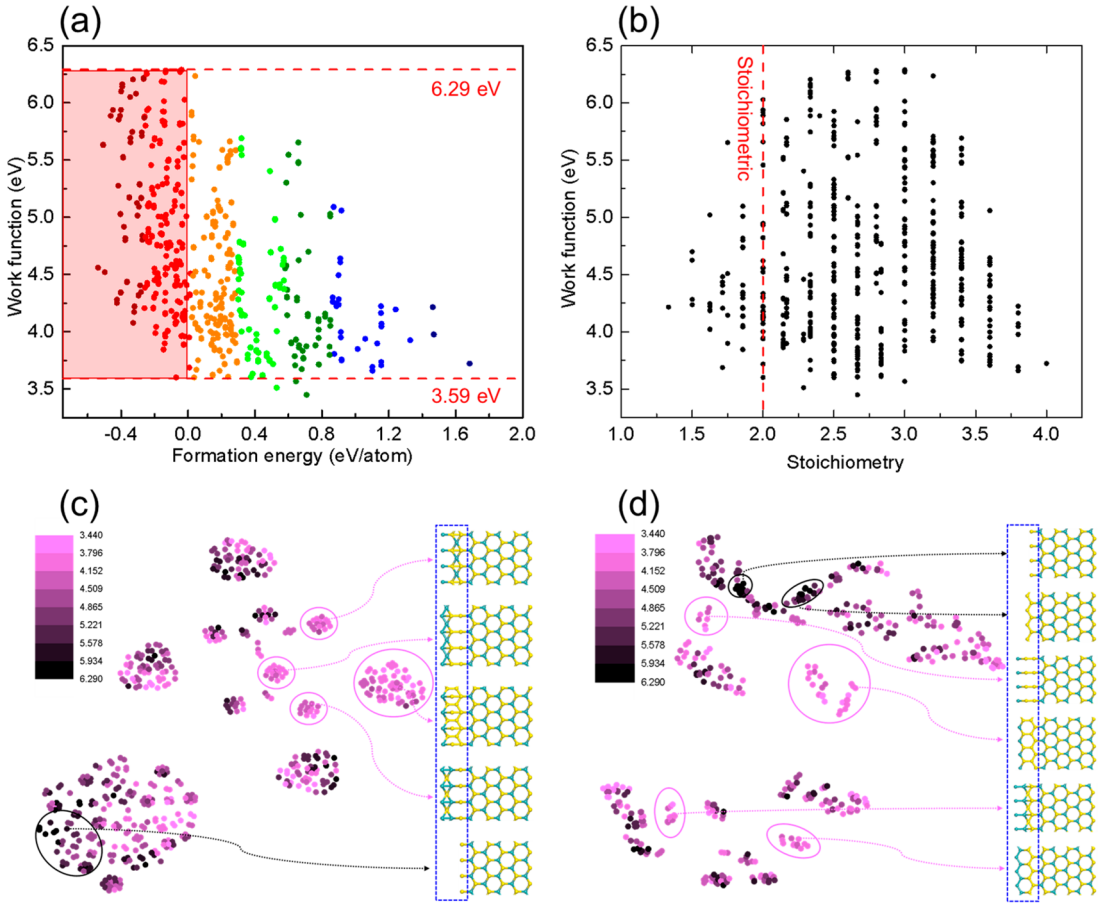

Figure 4. (a) Work function as a function of the formation energy for the 625 nanoribbons. Different colors of data points are assigned based on their formation energies. Data points for 267 thermodynamically stable reconstructed edges are enclosed in the red box. (b) Work function as a function of the stoichiometry for the 625 nanoribbons. Stoichiometric structures where S:Mo = 2 are indicated by a vertical dotted line. (c) The t-SNE plot of the atom-counting representation (with points color-coded by work function). (d) The t-SNE plot of the state-of-the-art many-body tensor representation (MBTR).

computed the formation energies. We find 267 reconstructed edges are thermodynamically stable (highlighted in a red box in Figure 4a), and these stable edges possess work functions spreading from 3.59 to 6.29 eV, with no discernible relation between the two quantities. Furthermore, no correlation could be found by plotting the stoichiometry versus work function (Figure 4b). The absence of a correlation between either stability or composition with the work function suggests additional influences, possibly from the geometric configurations of the edges. To investigate this, we compute structural features of the 2D MoS_2 and analyze them with t-SNE, a well-established method for mapping high-dimensional data.[37] We start by using a simple atom-counting representation, where each edge is represented by four values each representing a layer of the edge region. Within each layer, the Mo and S atoms are summed by their formal charges +4 and −2, respectively. The t-SNE plot of the atom-counting representation in Figure 4c (with points color-coded by work function) shows a surprisingly clear clustering of structures for many low work function cases, which are circled in pink. These clusters are grouped for their structural similarity and are characterized by edges with terminal Mo atoms and S underneath. The clustering is less clear for high work function cases. We next turn to a state-of-the-art representation using many-body tensors in Figure 4d, which incorporate a much higher degree of structural fidelity in the features.[38] Once again, similar groupings of low work function cases with terminal Mo with a high concentration of subedge S can be seen. Additionally, groups of high work function edges can also be identified, which all feature terminal S atoms with Mo directly underneath. These results are consistent with the prior observation that positively charged Mo at the edge leads to a low work function, as the presence of multiple coordinating S below the Mo edge is responsible for withdrawing the charge from Mo.

We next seek to derive the correlation of work function and edge property more strictly. If the direction along the width of the ribbon is set as y, the plane-averaged charge density $\rho(y)$ can be written as

$$\rho(y) = \frac{1}{A}\int \mathrm{d}x \int \mathrm{d}z \rho(\mathrm{x}, \mathrm{y}, \mathrm{z}) \tag{1}$$

where A is the area of the ribbon in the xz plane. Then the edge dipole moment can be calculated from this plane-averaged charge density as its first moment:

$$P = \int_{b_0}^{b} y\rho(y)\mathrm{d}y = \frac{-\varepsilon}{A}\int_{b_0}^{b} y\left(\frac{\partial^2 \mathrm{V}(\mathrm{y})}{\partial y^2}\right)\mathrm{d}y \tag{2}$$

Here the Poisson's equation was used to relate the plane-averaged electronic charge density to the plane-averaged potential $V(y)$, defined as

https://dx.doi.org/10.1021/acs.jpclett.1c00278
J. Phys. Chem. Lett. 2021, 12, 2320−2326

$$V(y) = \frac{1}{A}\int dx \int dz V(x, y, z) \tag{3}$$

In our calculations, the center of the ribbon was set as b_0, and b corresponds to the center of the vacuum in the supercell. Integrating by parts, we obtain the relation between the dipole moment and the plane-averaged potential to be

$$\frac{P}{\varepsilon} = \int_{b_0}^{b} dV(y) = V(b) - V(b_0) \tag{4}$$

If the value of the Fermi level (E_F) is set equal to zero, $-eV(b)$ is equal to the edge work function; therefore

$$W = -eV(b_0) - \frac{eP}{\varepsilon} \tag{5}$$

This expression is similar to that of 3D materials,[39] but it is now shown to be valid for edges, relating the work function explicitly to the edge dipole moment. We can clearly see a larger dipole moment will result in a smaller work function. To see this explicitly in our calculations, we can plot the work function versus the dipole moment. To eliminate the ambiguity in the choice of b_0, we plot the difference between W and W_0, where W_0 is the work function of the pristine Mo edge, which becomes

$$W - W_0 = -\frac{e(P - P_0)}{\varepsilon} \tag{6}$$

where P_0 is the dipole moment of the pristine edge. Equation 6 demonstrates that the change in the work function will be proportional to the change in the edge dipole moment. We thus understand the tunability of the work function in 2D nanoribbon edges to arise from intrinsic changes in the in-plane polarization due to edge reconstruction, in the limit that the two edges of a nanoribbon do not interact with each other (valid for wide nanoribbons such as ours as shown in Figure 2a).

In Figure 5, we plot the change in the work function ($W - W_0$) versus the change in the edge dipole moment ($P - P_0$) for

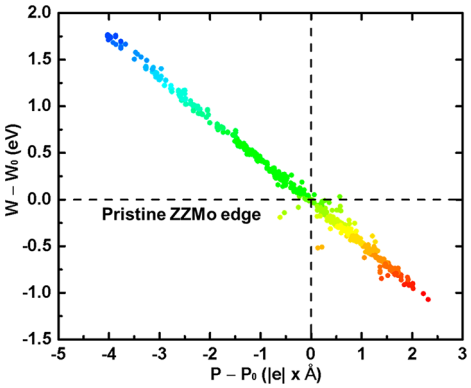

Figure 5. Linear correlations between the change in the work function ($W - W_0$) and the change in the edge dipole moment ($P - P_0$) at the Mo side. Different colors of data points are assigned based on their work function.

the 625 nanoribbons. The work function was computed by comparing the vacuum level with the Fermi level for each ribbon, and the edge dipole moment was computed by eq 2. A linear correlation between the change in the work function and the change in the dipole moment was observed. To guarantee that a reconstructed edge with specific work function is stable, we have replotted Figure 5 with only the 267 stable edges. As shown in Figure S2, a linear correlation with less scattering was observed for the stable edges. This is similar to 3D metals,[39] but here it is demonstrated for the first time to hold true in the 2D limit for nanoribbons. We have established that in the 2D limit the change in the work function is related to the change in the intrinsic polarization. Where does this change in polarization come from? From eq 2, it is known that the polarization is the first moment of the charge density, and therefore, the change in the charge density is the main cause. Figure S3 shows the charge density difference plots for ZZMo-S4 as an example. First, it confirms that the S side is not affected by the edge reconstruction at the Mo side. Second, the charge depletion on the outmost S atoms explains the relatively low work function of ZZMo-S4 (4.34 eV).

Compared to the previous method, the predominant advantage of edge reconstructions studied in the present work is the large tunability of the work function for 2D materials. Edge reconstructions can achieve a tunability of about 2.7 eV, while external doping, immersing into solutions, and varying the environment can so far modify the work function by only about 0.5 eV. In addition, edge reconstructions allow people to tune the work function in 2D materials intrinsically based on only the two constituent elements, as opposed to the conventional Edisonian manner of using extrinsic dopants or overlayers. With the large tunability of the work function, the performance of 2D materials can be further improved. For example, the MoS_2 nanoribbon with metallic edge can be treated as a metal like graphene, and it can be combined with n-Si to form a Schottky barrier solar cell. Ideally the open-circuit voltage, as well as short-circuit current and power conversion efficiency will increase as the work function and Schottky barrier height increase.[40] The output characteristics of the photovoltaic device will also be affected by other factors such as the carrier concentration and resistance of the edges. Nonetheless, there is a direct influence of work function on the performance which provides a strong motivation for work function tuning.

Our study of the work function in 2D MoS_2 presents several important implications. First, it indicates that 2D thin films with vertically aligned layers, thereby maximally exposing the edge sites, have different work function from their laterally aligned counterparts exposing the basal planes. In addition, the vertically aligned layers with different edge terminations will also have distinct work functions and functional properties. For example, the photoelectric effect would be different on different edges, and so would be the thermionic emission for these metallic nanoribbons with different edges. In our current model, the interaction between nearby nanoribbons was not considered. A previous study shows that MoS_2 nanoribbons with pristine edges are held together through weak vdW interaction with no strong interactions between the neighboring nanoribbons.[41] However, interactions between nanoribbons with reconstructed edges and how that affects the work functions at the edges are of great interest to be investigated in the future. Our study also implies that band offsets will be different at the two different edges in 2D lateral heterostructured devices, consequentially affecting electron transport through the nanoribbon. Thus, combining vertical and lateral 2D heterostructures, which show different interface electronic properties, and can lead to unique applications.[42] Second, it is known that the work function is a critical parameter for

https://dx.doi.org/10.1021/acs.jpclett.1c00278
J. Phys. Chem. Lett. 2021, 12, 2320−2326

catalysis, and therefore, reconstructed edges, which possess a wide range of work function, are promising catalyst candidates for various reactions such as hydrogen evolution reaction (HER),[43] oxygen reduction reactions (ORR) in fuel cells,[44] and hydrodesulfurization in the petroleum industry.[45,46] For example, it is shown that the catalytic activities of TMDC edges for CO_2 reduction increase as the work function decreases.[47,48] Thus, reconstructed edges which have lower work functions than the pristine edge can be more active for CO_2 reduction. Last but not least, because the change in the work function is linearly correlated to the change in edge dipole moment, it is expected that the dipole moment could be a promising new type of catalytic descriptor. Indeed, a recent machine learning study has demonstrated that a dipole-related descriptor can be used to accurately predict the key parameters of surface−molecular adsorbate interactions such as molecular adsorption energy and transferred charge.[49]

To summarize, we have investigated the work function of 2D MoS_2. We find that for a MoS_2 nanoribbon with metallic zigzag edges, the work function is 5.34 eV along the normal direction, while 4.45 eV (Mo side) and 5.87 eV (S side) along the in-plane direction, indicating that the work function of 2D MoS_2 could also be anisotropic like 3D materials that display surface-dependent work functions. By examing 625 MoS_2 nanoribbons with reconstructed edges at the Mo side, we find that the work function can be dramatically modified by edge reconstuctions. A wide and continuous range of work functions (from 3.59 to 6.29 eV) has been achieved within the 267 themodynamically stable edge configurations, making them promising for applications such as electron emitters, photovoltaic devices, and electrocatalysts. Finding no discernible relationship between stability or stoichiometry with the work function, we map out the 625 nanoribbons based on structural features and find the work function could be closely related to the presence of positive Mo or negative S at the edges. We derive the edge dipole moment as a key quantity which captures the charge distributions of the edge atoms and which directly correlates to the work function. Our work elucidates and numerically demonstrates for the first time the anisotropy of the work function in 2D materials and paves the way to effectively tune the work function without external doping.

■ ASSOCIATED CONTENT

Supporting Information

The Supporting Information is available free of charge at https://pubs.acs.org/doi/10.1021/acs.jpclett.1c00278.

Computational methods, histograms of the work function for the S side and normal direction, linear correlations for the 267 stable edges, edge reconstruction induced charge density difference, and test of the convergence of vacuum thickness (PDF)

■ AUTHOR INFORMATION

Corresponding Authors

Guoxiang Hu − *Center for Nanophase Materials Sciences, Oak Ridge National Laboratory, Oak Ridge, Tennessee 37831, United States; Department of Chemistry and Biochemistry, Queens College of the City University of New York, Queens, New York 11367, United States;* orcid.org/0000-0003-2942-8564; Email: guoxiang.hu@qc.cuny.edu

P. Ganesh − *Center for Nanophase Materials Sciences, Oak Ridge National Laboratory, Oak Ridge, Tennessee 37831, United States;* orcid.org/0000-0002-7170-2902; Email: ganeshp@ornl.gov

Authors

Victor Fung − *Center for Nanophase Materials Sciences, Oak Ridge National Laboratory, Oak Ridge, Tennessee 37831, United States;* orcid.org/0000-0002-3347-6983

Jingsong Huang − *Center for Nanophase Materials Sciences, Oak Ridge National Laboratory, Oak Ridge, Tennessee 37831, United States;* orcid.org/0000-0001-8993-2506

Complete contact information is available at: https://pubs.acs.org/10.1021/acs.jpclett.1c00278

Notes

The authors declare no competing financial interest.

■ ACKNOWLEDGMENTS

This research was conducted at the Center for Nanophase Materials Sciences, which is a DOE Office of Science User Facility. This research used the resources of the National Energy Research Scientific Computing Center and of the Compute and Data Environment for Science (CADES) at ORNL, which are supported by the Office of Science of the U.S. DOE under Contract Nos. DE-AC02-05CH11231 and DE-AC05-00OR22750, respectively.

■ REFERENCES

(1) Mas-Balleste, R.; Gomez-Navarro, C.; Gomez-Herrero, J.; Zamora, F. 2D Materials: To Graphene and Beyond. *Nanoscale* **2011**, *3*, 20−30.

(2) Gupta, A.; Sakthivel, T.; Seal, S. Recent Development in 2D Materials Beyond Graphene. *Prog. Mater. Sci.* **2015**, *73*, 44−126.

(3) Novoselov, K.; Mishchenko, A.; Carvalho, A.; Castro Neto, A. 2D Materials and Van der Waals Heterostructures. *Science* **2016**, *353*, aac9439.

(4) Hirsch, A.; Hauke, F. Post-Graphene 2D Chemistry: The Emerging Field of Molybdenum Disulfide and Black Phosphorus Functionalization. *Angew. Chem., Int. Ed.* **2018**, *57*, 4338−4354.

(5) Nichols, B.; Mazzoni, A.; Chin, M.; Shah, P.; Najmaei, S.; Burke, R.; Dubey, M. *Semiconductors and Semimetals*; Elsevier, 2016.

(6) Gibertini, M.; Koperski, M.; Morpurgo, A.; Novoselov, K. Magnetic 2D Materials and Heterostructures. *Nat. Nanotechnol.* **2019**, *14*, 408−419.

(7) Yu, S.; Wu, X.; Wang, Y.; Guo, X.; Tong, L. 2D Materials for Optical Modulation: Challenges and Opportunities. *Adv. Mater.* **2017**, *29*, 1606128.

(8) Deng, D.; Novoselov, K.; Fu, Q.; Zheng, N.; Tian, Z.; Bao, X. Catalysis with Two-Dimensional Materials and Their Heterostructures. *Nat. Nanotechnol.* **2016**, *11*, 218−230.

(9) Kahn, A. Fermi Level, Work Function and Vacuum Level. *Mater. Horiz.* **2016**, *3*, 7−10.

(10) Cahen, D.; Kahn, A. Electron Energetics at Surfaces and Interfaces: Concepts and Experiments. *Adv. Mater.* **2003**, *15*, 271−277.
(11) Ye, K. H.; Li, H.; Huang, D.; Xiao, S.; Qiu, W.; Li, M.; Hu, Y.; Mai, W.; Ji, H.; Yang, S. Enhancing Photoelectrochemical Water Splitting by Combining Work Function Tuning and Heterojunction Engineering. *Nat. Commun.* **2019**, *10*, 3687.
(12) Sharma, M.; Jang, J. H.; Shin, D. Y.; Kwon, J. A.; Lim, D. H.; Choi, D.; Sung, H.; Jang, J.; Lee, S. Y.; Lee, K. Y.; et al. Work Function-Tailored Graphene via Transition Metal Encapsulation as a Highly Active and Durable Catalyst for the Oxygen Reduction Reaction. *Energy Environ. Sci.* **2019**, *12*, 2200−2211.
(13) Agresti, A.; Pazniak, A.; Pescetelli, S.; Di Vito, A.; Rossi, D.; Pecchia, A.; der Maur, M. A.; Liedl, A.; Larciprete, R.; Kuznetsov, D. V.; et al. Titanium-Carbide Mxenes for Work Function and Interface Engineering in Perovskite Solar Cells. *Nat. Mater.* **2019**, *18*, 1228−1234.
(14) Yu, Y. J.; Zhao, Y.; Ryu, S.; Brus, L. E.; Kim, K. S.; Kim, P. Tuning the Graphene Work Function by Electric Field Effect. *Nano Lett.* **2009**, *9*, 3430−3434.
(15) Park, J.; Lee, W. H.; Huh, S.; Sim, S. H.; Kim, S. B.; Cho, K.; Hong, B. H.; Kim, K. S. Work-Function Engineering of Graphene Electrodes by Self-Assembled Monolayers for High-Performance Organic Field-Effect Transistors. *J. Phys. Chem. Lett.* **2011**, *2*, 841−845.
(16) Zhou, Y.; Fuentes-Hernandez, C.; Shim, J.; Meyer, J.; Giordano, A. J.; Li, H.; Winget, P.; Papadopoulos, T.; Cheun, H.; Kim, J. A.; et al. Universal Method to Produce Low−Work Function Electrodes for Organic Electronics. *Science* **2012**, *336*, 327−332.
(17) Lee, W. H.; Park, Y. D. Tuning Electrical Properties of 2D Materials by Self-Assembled Monolayers. *Adv. Mater. Interfaces* **2018**, *5*, 1700316.
(18) Shi, Y.; Kim, K. K.; Reina, A.; Hofmann, M.; Li, L. J.; Kong, J. Work Function Engineering of Graphene Electrode via Chemical Doping. *ACS Nano* **2010**, *4*, 2689−2694.
(19) Lee, S. Y.; Kim, U. J.; Chung, J.; Nam, H.; Jeong, H. Y.; Han, G. H.; Kim, H.; Oh, H. M.; Lee, H.; Kim, H.; et al. Large Work Function Modulation of Monolayer MoS_2 by Ambient Gases. *ACS Nano* **2016**, *10*, 6100−6107.
(20) Bardeen, J. Theory of the Work Function. II. The Surface Double Layer. *Phys. Rev.* **1936**, *49*, 653−663.
(21) Lang, N.; Kohn, W. Theory of Metal Surfaces: Work Function. *Phys. Rev. B* **1971**, *3*, 1215−1223.
(22) Smoluchowski, R. Anisotropy of the Electronic Work Function of Metals. *Phys. Rev.* **1941**, *60*, 661−674.
(23) Zhong, Z.; Hansmann, P. Tuning the Work Function in Transition Metal Oxides and Their Heterostructures. *Phys. Rev. B: Condens. Matter Mater. Phys.* **2016**, *93*, 235116.
(24) Zhao, X.; Fu, D.; Ding, Z.; Zhang, Y. Y.; Wan, D.; Tan, S. J.; Chen, Z.; Leng, K.; Dan, J.; Fu, W.; et al. Mo-Terminated Edge Reconstructions in Nanoporous Molybdenum Disulfide Film. *Nano Lett.* **2018**, *18*, 482−490.
(25) Sang, X.; Li, X.; Zhao, W.; Dong, J.; Rouleau, C. M.; Geohegan, D. B.; Ding, F.; Xiao, K.; Unocic, R. R. In Situ Edge Engineering in Two-Dimensional Transition Metal Dichalcogenides. *Nat. Commun.* **2018**, *9*, 2051.
(26) Hu, G.; Fung, V.; Sang, X.; Unocic, R. R.; Ganesh, P. Predicting Synthesizable Multi-Functional Edge Reconstructions in Two-Dimensional Transition Metal Dichalcogenides. *npj Comput. Mater.* **2020**, *6*, 44.
(27) Hu, G.; Fung, V.; Sang, X.; Unocic, R. R.; Ganesh, P. Superior Electrocatalytic Hydrogen Evolution at Engineered Non-Stoichiometric Two-Dimensional Transition Metal Dichalcogenide Edges. *J. Mater. Chem. A* **2019**, *7*, 18357−18364.
(28) Li, H.; Wu, H.; Yuan, S.; Qian, H. Synthesis and Characterization of Vertically Standing MoS_2 Nanosheets. *Sci. Rep.* **2016**, *6*, 21171.
(29) Cho, S. Y.; Kim, S. J.; Lee, Y.; Kim, J. S.; Jung, W. B.; Yoo, H. W.; Kim, J.; Jung, H. T. Highly Enhanced Gas Adsorption Properties in Vertically Aligned MoS_2 Layers. *ACS Nano* **2015**, *9*, 9314−9321.
(30) Kong, D.; Wang, H.; Cha, J. J.; Pasta, M.; Koski, K. J.; Yao, J.; Cui, Y. Synthesis of MoS_2 and $MoSe_2$ Films with Vertically Aligned Layers. *Nano Lett.* **2013**, *13*, 1341−1347.
(31) Wang, H.; Lu, Z.; Xu, S.; Kong, D.; Cha, J. J.; Zheng, G.; Hsu, P.-C.; Yan, K.; Bradshaw, D.; Prinz, F. B.; et al. Electrochemical Tuning of Vertically Aligned MoS_2 Nanofilms and Its Application in Improving Hydrogen Evolution Reaction. *Proc. Natl. Acad. Sci. U. S. A.* **2013**, *110*, 19701−19706.
(32) Son, Y. W.; Cohen, M. L.; Louie, S. G. Energy Gaps in Graphene Nanoribbons. *Phys. Rev. Lett.* **2006**, *97*, 216803.
(33) Li, X.; Wang, X.; Zhang, L.; Lee, S.; Dai, H. Chemically Derived, Ultrasmooth Graphene Nanoribbon Semiconductors. *Science* **2008**, *319*, 1229−1232.
(34) Chen, Y. C.; Cao, T.; Chen, C.; Pedramrazi, Z.; Haberer, D.; De Oteyza, D. G.; Fischer, F. R.; Louie, S. G.; Crommie, M. F. Molecular Bandgap Engineering of Bottom-up Synthesized Graphene Nanoribbon Heterojunctions. *Nat. Nanotechnol.* **2015**, *10*, 156−160.
(35) Li, D.; Ding, F. Environment-Dependent Edge Reconstruction of Transition Metal Dichalcogenides: A Global Search. *Mater. Today Adv.* **2020**, *8*, 100079.
(36) Lauritsen, J. V.; Nyberg, M.; Vang, R. T.; Bollinger, M.; Clausen, B.; Topsøe, H.; Jacobsen, K. W.; Lægsgaard, E.; Nørskov, J.; Besenbacher, F. Chemistry of One-Dimensional Metallic Edge States in MoS_2 Nanoclusters. *Nanotechnology* **2003**, *14*, 385−389.
(37) Maaten, L. V. D.; Hinton, G. Visualizing Data Using T-SNE. *J. Mach. Learn. Res.* **2008**, *9*, 2579−2605.
(38) Huo, H.; Rupp, M.. Unified Representation of Molecules and Crystals for Machine Learning. *arXiv* **2017**, 1704.06439.
(39) Leung, T.; Kao, C.; Su, W.; Feng, Y.; Chan, C. Relationship between Surface Dipole, Work Function and Charge Transfer: Some Exceptions to an Established Rule. *Phys. Rev. B: Condens. Matter Mater. Phys.* **2003**, *68*, 195408.
(40) Ponpon, J.; Siffert, P. Open-Circuit Voltage of MIS Silicon Solar Cells. *J. Appl. Phys.* **1976**, *47*, 3248−3251.
(41) Li, Y.; Zhou, Z.; Zhang, S.; Chen, Z. MoS_2 Nanoribbons: High Stability and Unusual Electronic and Magnetic Properties. *J. Am. Chem. Soc.* **2008**, *130*, 16739−16744.
(42) Gong, Y.; Lin, J.; Wang, X.; Shi, G.; Lei, S.; Lin, Z.; Zou, X.; Ye, G.; Vajtai, R.; Yakobson, B. I.; et al. Vertical and In-Plane Heterostructures from WS_2/MoS_2 Monolayers. *Nat. Mater.* **2014**, *13*, 1135−1142.
(43) Jaramillo, T. F.; Jørgensen, K. P.; Bonde, J.; Nielsen, J. H.; Horch, S.; Chorkendorff, I. Identification of Active Edge Sites for Electrochemical H_2 Evolution from MoS_2 Nanocatalysts. *Science* **2007**, *317*, 100−102.
(44) Ahmed, S. M.; Gerischer, H. Influence of Crystal Surface Orientation on Redox Reactions at Semiconducting MoS_2. *Electrochim. Acta* **1979**, *24*, 705−711.
(45) Prins, R.; De Beer, V.; Somorjai, G. Structure and Function of the Catalyst and the Promoter in Co-Mo Hydrodesulfurization Catalysts. *Catal. Rev.: Sci. Eng.* **1989**, *31*, 1−41.
(46) Byskov, L. S.; Nørskov, J. K.; Clausen, B. S.; Topsøe, H. DFT Calculations of Unpromoted and Promoted MoS_2-Based Hydrodesulfurization Catalysts. *J. Catal.* **1999**, *187*, 109−122.
(47) Asadi, M.; Kim, K.; Liu, C.; Addepalli, A. V.; Abbasi, P.; Yasaei, P.; Phillips, P.; Behranginia, A.; Cerrato, J. M.; Haasch, R.; et al. Nanostructured Transition Metal Dichalcogenide Electrocatalysts for CO_2 Reduction in Ionic Liquid. *Science* **2016**, *353*, 467−470.
(48) Asadi, M.; Kumar, B.; Behranginia, A.; Rosen, B. A.; Baskin, A.; Repnin, N.; Pisasale, D.; Phillips, P.; Zhu, W.; Haasch, R.; et al. Robust Carbon Dioxide Reduction on Molybdenum Disulphide Edges. *Nat. Commun.* **2014**, *5*, 4470.
(49) Wang, X.; Ye, S.; Hu, W.; Sharman, E.; Liu, R.; Liu, Y.; Luo, Y.; Jiang, J. Electric Dipole Descriptor for Machine Learning Prediction of Catalyst Surface-Molecular Adsorbate Interactions. *J. Am. Chem. Soc.* **2020**, *142*, 7737−7743.

https://dx.doi.org/10.1021/acs.jpclett.1c00278
J. Phys. Chem. Lett. 2021, 12, 2320−2326